Article

Chinese Science Bulletin

SPECIAL TOPIC
Plasmonics

August 2010 Vol.55 No.24: 2635–2642
doi: 10.1007/s11434-010-4044-0

FDTD for plasmonics: Applications in enhanced Raman spectroscopy

YANG ZhiLin[1*], LI QianHong[1], RUAN FangXiong[1], LI ZhiPeng[2], REN Bin[3], XU HongXing[2] & TIAN ZhongQun[3]

[1] *Department of Physics, Xiamen University, Xiamen 361005, China;*
[2] *Institute of Physics, Chinese Academy of Sciences, Beijing 100190, China;*
[3] *Department of Chemistry, Xiamen University, Xiamen 361005, China*

Received April 11, 2010; accepted June 7, 2010

The exact electromagnetic enhancement mechanism behind SERS, TERS, HERS and SHINERS is one of the issues focused on in the study of enhanced Raman spectroscopy. The three dimensional finite difference time domain method (3D-FDTD), which is widely used in nanoplasmonic simulations, not only provides us with a powerful numerical tool for theoretical studies of the ERS electromagnetic enhancement mechanism, but also serves as a useful tool for the design of ERS-active systems with higher sensitivities and spectral spatial resolution. In this paper, we first introduce the fundamental principles of FDTD algorithms, and then the size-dependent dielectric function of dispersive metallic material is discussed. A comparative study of FDTD and rigorous Mie evaluations of electromagnetic fields in the vicinity of a system of self-similar nanospheres shows an excellent correlation between the two computational methods, directly confirming the validity and accuracy of 3D-FDTD simulations in ERS calculations. Finally, we demonstrate, using a TERS calculation as an example, that the non-uniform mesh method can be more computationally efficient without loss of accuracy if it is applied correctly.

plasmonics, FDTD, SERS, TERS

Citation: Yang Z L, Li Q H, Ruan F X, et al. FDTD for plasmonics: Applications in enhanced Raman spectroscopy. Chinese Sci Bull, 2010, 55: 2635–2642, doi: 10.1007/ s11434-010-4044-0

Surface enhanced Raman spectroscopy (SERS) [1–3], tip-enhanced Raman spectroscopy (TERS) [4–6], hole-enhanced Raman spectroscopy (HERS) [7,8] and shell-isolated nanoparticle-enhanced Raman spectroscopy (SHINERS) [9] are the most popular forms of enhanced Raman spectroscopy (ERS). ERS has been employed and widely used as an important spectroscopic tool for sensitive and specific detection of chemical, biological, and medical analytes and is of great interest to many fields such as biology, medicine, nanoplasmonics, surface science, near field optics, environmental monitoring, as well as nanoscience and nanotechnology. The enhancement factors arising from ERS can be as large as 10 orders of magnitude or more, which allows the technique to be sensitive enough to detect single molecules. Due to the high detection sensitivity, enhanced Raman spectroscopy has been applied to *in situ* diagnostic probes for the study of the detailed molecular structure and orientation of surface species [10–18] since its discovery in 1974 [1].

The exact mechanism of ERS is still a matter of debate in the literature. Nowadays, it is generally accepted the there are two mechanisms which are jointly responsible for the majority of the SERS effect: Electromagnetic (EM) enhancement associated with large local fields caused by surface plasmon resonance and chemical enhancement involving a charge transfer (CT) process associated with chemical interactions between a molecule and a metal particle or surface. The EM mechanism, initially proposed by Moskovits

*Corresponding author (email: zlyang@xmu.edu.cn)

in 1978 [19], immediately led to a number of predictions. One of these predictions stated that SERS should be observable in all plasmonic metal colloids with silver providing the most intense SERS signal at visible wavelengths, followed by gold and copper. This was shown to be true and, additionally, some other predictions such as polarization, excitation, and size and shape dependence were found to be in qualitative agreement with the surface plasmon based theory. When EM theory is applied to aggregates of particles, it also makes the reason understandable that SERS can provide single-molecule sensitivity. Although EM theory still cannot fully explain ERS and the relative importance of the EM and chemical enhancement remains ambiguous, it is generally accepted that the EM effect plays a dominant role since the chemical enhancement will never, even under the best experimental conditions, exceed two orders of magnitude.

A series of breakthroughs in the past decades have provided us with an important opportunity to explore the complex and controversial EM mechanism of ERS. Everything that has been learned regarding single molecular SERS (SM-SERS) [13–15], SERS from transition metals (TM-SERS) [16], HERS [7,8,20], TERS [4–6,17,18] and SHINERS [9] has led scientists to believe that ERS is not a single particle effect. An efficient ERS-active system is strongly dependent on the particle-particle, particle-substrate or tip-substrate near-field coupling effect [15,21,22]. Therefore, the research model for the EM enhancement mechanism of ERS has changed its focus from highly symmetric isolated particles to particle aggregates of arbitrary size and shape. The near field coupling effect, which is the origin of the "hot site" or "hot particle", has received unprecedented attention over the past ten years.

To perform electrodynamic calculations of light scattering from complex ERS-active systems, especially in the study of 'hot particle' and 'hot spot' formation and enhancement, one has to solve the Maxwell equations accurately. Mie theory, the only analytical method to solve Maxwell's equations completely [23], is the most fundamental tool to deal with the problem of light scattering from spherical particles. We can easily solve for the optical properties, such as extinction efficiency and near field distribution, of a given illuminated nanosphere or nanosphere aggregate through Mie calculations if the size, dielectric function and environmental medium of the particle are known. Because of its accuracy and unambiguous physical meaning of the calculation results, Mie theory is necessarily recognized as the most important standard by which the reliability and accuracy of any newly developed numerical calculation method can be tested. However, the application of Mie theory is strictly limited to spherical particles and, thus, cannot be used for the quantitative calculation of EM enhancement factors in ERS systems that consist of non-spherical particles, tips or substrates. In order to determine the electromagnetic fields around multiple nanostructures of more complex geometries, for example, an ERS system with non-spherical particles or tips, it becomes necessary to employ a numerical method technique. Several numerical methods, including finite difference time domain (FDTD) [24–28], finite element method (FEM) [29,30], boundary element method (BEM) [31,32], and discrete dipole approximation (DDA) [33,34] have been proposed for determining the electromagnetic fields around individual non-spherical metallic nanoparticles as well as nanoparticles arrays in enhanced spectroscopy. These numerical methods have achieved great successes in simulating the near field coupling effect in SM-SERS, TERS, HERS and SHINERS. Among these methods, the three dimensional FDTD (3D-FDTD) method is one of the most popular tools used to simulate the distribution of the electromagnetic field around the illuminated nanoparticles, tips and substrates in an ERS system with arbitrary geometry. Because FDTD method provides a convenient, systematic and general approach for calculating the optical response of plasmonic nanostructures of arbitrary symmetry and geometry to an incident light wave, it has been successfully and widely used in various areas of plasmonics research such as plasmon waveguides, extraordinary optical transmission (EOT) through sub-wavelength apertures, surface-plasmon-polariton-based sensors, enhanced optical absorption and scattering, metamaterials and imaging, plasmonic nanolithography, etc. [35–39]. In this paper, we shall begin by briefly introducing the basic principles of FDTD and its applications in dispersive materials where the size-dependent dielectric function of metallic nanoparticles is discussed as an indispensable background. Next, we illustrate and confirm the validity and accuracy of 3D-FDTD simulations in ERS calculations by comparing the FDTD results with rigorous Mie theory. Finally, taking TERS as an example, a non-uniform mesh method in 3D-FDTD and its applications is described and discussed.

1 FDTD basics

The FDTD approach has rapidly become one of the most important computational methods in electromagnetics since Yee proposed it in 1966 [40]. In the FDTD approach, both space and time are divided into discrete segments. Space is segmented into box-shaped "cells" with the electric fields located on the edges of the box and the magnetic fields positioned on the faces. Every E component is surrounded by four H components and every H component is surrounded by four E components. This orientation of the fields is known as the "Yee cell", which is the basis for any FDTD simulation. Time is quantized into small steps where each step represents the time required for the field to travel from one cell to the next. The FDTD method involves the discretization of Maxwell's equations in both the time and the space domain in order to find the E and H fields at different

positions and at different time-steps. The FDTD method can conveniently be applied to simulating the electromagnetic scattering and radiation from a target of complex shape as well as non-uniform dielectric objects by simply adjusting the number, size and material properties of the Yee cell [41].

The basic principle of FDTD is to numerically solve Maxwell's differential equations:

$$\nabla \times \vec{E} = -\frac{\partial \vec{B}}{\partial t}, \tag{1}$$

$$\nabla \times \vec{H} = \vec{J} + \frac{\partial \vec{D}}{\partial t}, \tag{2}$$

where $\vec{E}$, $\vec{D}$, $\vec{H}$, $\vec{B}$, $\vec{J}$ represent the electric field, electric displacement, magnetic field, magnetic induction intensity and current density, respectively. For isotropic media, the relationship between these physical quantities is

$$\vec{D} = \varepsilon \vec{E},\ \vec{B} = \mu \vec{H},\ \vec{J} = \sigma \vec{E}, \tag{3}$$

where ε,μ,σ are the medium dielectric constant, magnetic permeability coefficient and electrical conductivity, respectively. In a rectangular coordinate system, eqs. (l) and (2) are equivalent to the following scalar equations:

$$\frac{\partial E_z}{\partial y} - \frac{\partial E_y}{\partial z} = -\mu \frac{\partial H_x}{\partial t}, \tag{4}$$

$$\frac{\partial E_x}{\partial z} - \frac{\partial E_z}{\partial x} = -\mu \frac{\partial H_y}{\partial t}, \tag{5}$$

$$\frac{\partial E_y}{\partial x} - \frac{\partial E_x}{\partial y} = -\mu \frac{\partial H_z}{\partial t}, \tag{6}$$

$$\frac{\partial H_z}{\partial y} - \frac{\partial H_y}{\partial z} = \varepsilon \frac{\partial E_x}{\partial t} + \sigma E_x, \tag{7}$$

$$\frac{\partial H_x}{\partial z} - \frac{\partial H_z}{\partial x} = \varepsilon \frac{\partial E_y}{\partial t} + \sigma E_y, \tag{8}$$

$$\frac{\partial H_y}{\partial x} - \frac{\partial H_x}{\partial y} = \varepsilon \frac{\partial E_z}{\partial t} + \sigma E_z. \tag{9}$$

Taking that function $f(x,y,z,t)$ denotes the electric or magnetic field in the coordinate system, we have the form $f(x,y,z,t)=f(i\Delta x,j\Delta y,k\Delta z,n\Delta t)=f^n(i,j,k)$.Then $f(x,y,z,t)$ can be discretized via the central difference approximation in both space and time:

$$\left.\frac{\partial f(x,y,z,t)}{\partial x}\right|_{x=i\Delta x} \approx \frac{f^n(i+\frac{1}{2},j,k) - f^n(i-\frac{1}{2},j,k)}{\Delta x}, \tag{10}$$

$$\left.\frac{\partial f(x,y,z,t)}{\partial y}\right|_{y=j\Delta y} \approx \frac{f^n(i,j+\frac{1}{2},k) - f^n(i,j-\frac{1}{2},k)}{\Delta y}, \tag{11}$$

$$\left.\frac{\partial f(x,y,z,t)}{\partial z}\right|_{z=k\Delta z} \approx \frac{f^n(i,j,k+\frac{1}{2}) - f^n(i,j,k-\frac{1}{2})}{\Delta z}, \tag{12}$$

$$\left.\frac{\partial f(x,y,z,t)}{\partial t}\right|_{t=n\Delta t} \approx \frac{f^{n+\frac{1}{2}}(i,j,k) - f^{n-\frac{1}{2}}(i,j,k)}{\Delta t}. \tag{13}$$

This sampling method of the electromagnetic field components in the Yee cell is propitious to the differential calculation of Maxwell's equations, and it is consistent with Faraday's law of electromagnetic induction.

In order to obtain an accurate field distribution for the studied object, the Yee cell size, the most important constraint in an FDTD simulation, must be significantly smaller than the smallest excitation wavelength. An often quoted constraint is "ten cells per wavelength", which means the side of each cell should be 1/10λ or less than the shortest wavelength of interest. Another cell size consideration is that the important characteristics of the object geometry must be accurately modeled. In general ERS cases, the latter constraint is often more decisive since most of the ERS active geometry is in the range of ten to hundreds of nanometers. In general, the smaller the Yee cell size, the better the calculation results. However, due to the limitation of computation resources, cell size cannot, for practical purposes, be infinitely small. The cell size selected for a given simulation must take both the available computational resources and requisite calculation accuracy into consideration. For enhanced Raman spectroscopy system, the cell size is usually in the range of 1 to 2 nanometers or less. This means that an FDTD calculation for ERS is often a time-consuming task. As a result, we sometimes have to fall back on the non-uniform FDTD mesh method to save computation resources and calculation time.

2 Dealing with the dielectric functions of metallic materials in FDTD

The method used to deal with dispersive materials in FDTD is of great importance for ERS simulations since the complex permittivity of the metals in the optical frequency range is strongly frequency dependent. Benefiting from the method developed by Leubbers, Hunsberger and Kunz, it has been possible to use an FDTD method based on the simple Drude model for these dispersive materials since the early 1990s [42,43]. Although the Drude model of the FDTD algorithm achieved some success, the dielectric constant of actual metal over a wide frequency range is difficult to simulate accurately using the simple free-electron gas model and, furthermore, the Fourier transform of the polarization used in the algorithm often leads to instability in the calculation. Here, instead of the simple Drude model, we adopt the general Drude model (modified Debye model) to simulate the complex permittivity with the form of

[24,27,44]:

$$\varepsilon(\omega)=\varepsilon_{\infty}+\frac{\varepsilon_{\mathrm{s}}-\varepsilon_{\infty}}{1+i\omega\tau}+\frac{\sigma}{i\omega\varepsilon_0}. \tag{14}$$

This equation can be expanded into two equations to denote the real and imaginary parts of the dielectric constant respectively:

$$\varepsilon_{\mathrm{r}}=\varepsilon_{\infty}+\frac{(\varepsilon_{\mathrm{s}}-\varepsilon_{\infty})}{1+\omega^2\tau^2}, \tag{15}$$

$$\varepsilon_{\mathrm{i}}=-\left[\frac{(\varepsilon_{\mathrm{s}}-\varepsilon_{\infty})\omega\tau}{1+\omega^2\tau^2}+\frac{\sigma}{\omega\varepsilon_0}\right], \tag{16}$$

where ε_{s}, ε_{∞}, σ, τ, ω, ε_0 represent the static permittivity, infinite frequency permittivity, conductivity, relaxation time, angular frequency and permittivity of free space, respectively. The four parameters ε_{s}, ε_{∞}, σ, τ can be adjusted through curve-fitting techniques to correctly match the complex permittivity which can be derived from the experimentally determined optical constants. It is important to keep in mind that for the general Drude model materials, the infinite frequency permittivity must meet the condition $\varepsilon_{\infty}\geqslant 1$ and the conductivity should obey the equation $\sigma \geqslant \frac{\varepsilon_0(\varepsilon_{\infty}-\varepsilon_{\mathrm{s}})}{\tau_0}$ if $\varepsilon_{\mathrm{s}}<\varepsilon_{\infty}$.

It should be pointed out here that the value of dielectric constants for a nanostructure may show great difference from that of bulk material if the size of the nanostructure used in ERS is smaller than the mean free path of the conduction electrons [45,46]. Since surface plasmon resonance, which determines the EM enhancement factor in ERS, is strongly dependent on the dielectric constants, it is necessary to discuss the size dependence of dielectric functions for metallic nanoparticles before performing FDTD simulations. In fact, it has been confirmed that small changes in the dielectric constant will result in significant changes in plasmonic calculation results [47,48].

The classical approach for describing the size dependence of the dielectric function assumes that if the particle size is comparable to or smaller than the mean free path of the conduction electrons in the bulk, the scattering of the conduction electrons from the particle surface will result in a reduced effective mean free path. For bulk metal materials, the damping that determines γ_0 is due to the scattering of the electrons from phonons, electrons, lattice defects or impurities, which can be expressed as [45]

$$\gamma_0=\frac{v_{\mathrm{f}}}{l_{\infty}}, \tag{17}$$

where v_{f} is the Fermi velocity and l_{∞} is the mean free path of the conduction electrons in the bulk. When the particle size is smaller than l_{∞}, the scattering of the conduction electrons from particle surface results in a reduced effective mean free path l_{eff} and increased γ through

$$\gamma=\gamma_0+A\frac{v_{\mathrm{f}}}{l_{\mathrm{eff}}}, \tag{18}$$

where A is a dimensionless parameter that includes details of the scattering process, usually assumed to be close to unity. The bound contribution to the dielectric function plays an important role in determining plasmon resonance wavelengths; however, the size dependence of the dielectric function is usually assumed to be determined by the free electron contribution. This leads to a correction to literature values of $\varepsilon_{\mathrm{bulk}}(\omega)$ given by

$$\varepsilon(\omega,l_{\mathrm{eff}})=\varepsilon_{\mathrm{bulk}}(\omega)+\frac{\omega_p^2}{\omega^2+i\omega\gamma_0}-\frac{\omega_p^2}{\omega^2+i\omega(\gamma_0+A\frac{v_{\mathrm{f}}}{l_{\mathrm{eff}}})}. \tag{19}$$

Figure 1 compares the bulk value of the dielectric function of silver with the dielectric function corrected by the mean free path approach for particles of different sizes. The bulk refractive index, extinction coefficient and the electron mean free path of silver used in the calculation are all taken from experimental data in the literature [49]. The size-dependent dielectric functions are then calculated using eq. (19). Figure 1(a) shows that the imaginary part of the dielectric constant of silver is significantly affected by the particle size, as its value increases rapidly when the particle size is decreased. When the particle size is reduced to 10 nm, the value of the imaginary component increases dramatically in comparison with that of bulk silver in the visible light range. Moreover, in the infrared region the size effect on the dielectric function is more obvious and changes in the imaginary part of the dielectric function have to be considered for silver particles as large as 100 nm. The increase in value of the imaginary component will result in a negative damping effect on both the SPR and SERS phenomena. On the other hand, the real part of the dielectric function of silver is less affected by the size effect, as shown in Figure 1(b). The real part of the dielectric function remains in good agreement with the bulk value throughout the entire visible light range. This remains true even for particles with radii as small as 5 nm, where only in the infrared range can a small deviation be seen.

3 Validity of FDTD

As a numerical method, it is necessary to judge and review the validity of the FDTD method before its application in enhanced Raman scattering simulations. For this purpose, we performed FDTD simulations and compared the results with rigorous Mie theory calculations for the same SERS system. The results are shown in Figure 2.

In the calculation, the field enhancement of a self-similar system composed of 3 silver nanospheres was studied; the

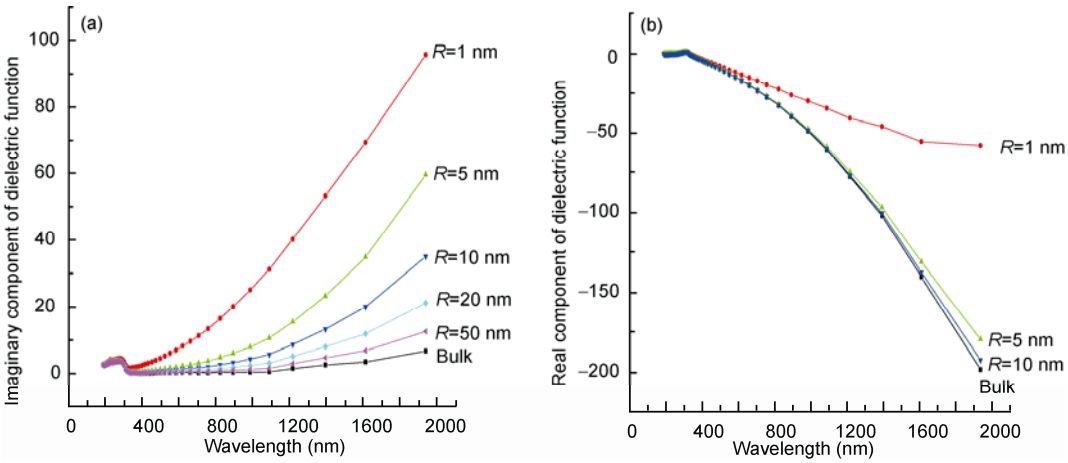

Figure 1 Comparison between the real and imaginary dielectric functions of bulk silver and silver particles of different sizes. (a) The dependence of the imaginary part of the dielectric function on nanoparticle size; (b) the dependence of the real part of the dielectric function on particle size.

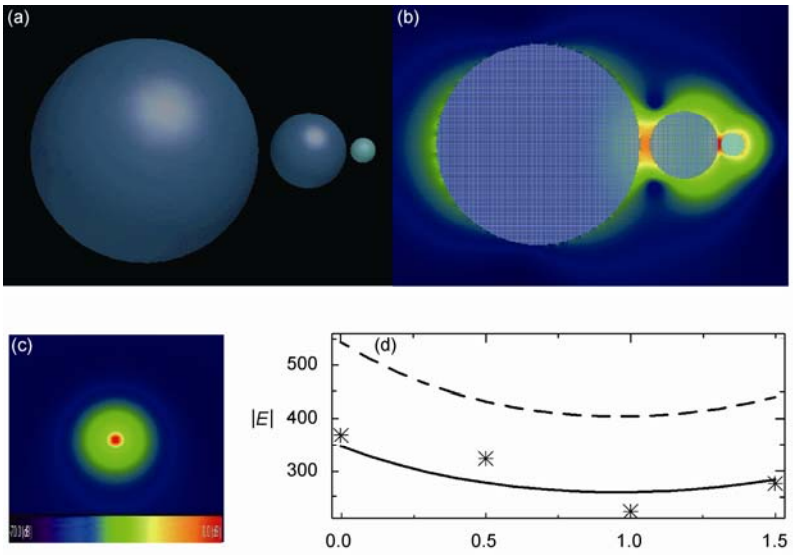

Figure 2 Validity of 3D-FDTD calculations in ERS. (a) Calculation model; (b) FDTD simulations of the electric-field distribution in the central plane through the axis; (c) electric-field distribution in the central gap plane (perpendicular to the symmetric axis) between the two smallest nanospheres; (d) the field enhancement distribution along the axis of symmetry between the two smallest spheres (starting from the smallest sphere) calculated by Mie theory (line) and FDTD (asterisks) respectively. The data in (d) are taken from [48].

calculation model is illustrated in Figure 2(a). The diameters of the three Ag spheres, from the left to right, are 90 nm, 30 nm and 10 nm, respectively, and the surface to surface gap distance is 4.5 nm and 1.5 nm, respectively. In the calculation, the wave vector of the 3.25 eV incident plane wave is perpendicular to the axis of symmetry, and the polarization is parallel to the axis of symmetry. This calculation model is taken from [50]. In the calculation, the dielectric functions of the 90 nm and 30 nm silver spheres are directly taken from the bulk dielectric function of Ag from [49]. However, for the 10 nm Ag sphere, the dielectric function adjusted according to eq. (19) since the scattering of the conduction electrons from the particle surface will result in a distinct reduced effective mean free path as aforementioned. Although the real part of the dielectric constant is not significantly affected by particle size, the imaginary part increases significantly from the bulk value of 0.2 to 0.6 for a 10 nm particle. The Yee cell size used in the 3D-FDTD simulation was set to be 0.5 nm × 0.5 nm × 0.5 nm, and the total number of time steps was set to be 21000 to ensure convergence, which could be judged by checking whether near zone electric field values had reached a steady state. Figure 2(b) vividly shows the FDTD simulated electric-field distribution in the central plane through the axis of the self-similar chain of nanospheres. Figrue 2(c) gives the electric-field distribution in the central gap plane (perpendicular to the symmetric axis) between the two smallest nanospheres. From Figure 2(b) and (c), we can see that the electric field enhancement in the studied plane can be directly calculated and visualized through FDTD simulations;

this is of great importance for EM mechanism studies of ERS. In the gap between the nanospheres, the maximum field enhancement is about 300, corresponding to ca. 9 to 10 orders SERS enhancement. The huge enhancement at the interparticle junction, which originates from the strong near field coupling effect, is directly related to the so-called "hot spot" phenomenon in single molecular SERS [15,21].

The distributions of field enhancement along the axis of symmetry between the two smallest spheres (beginning from the smallest sphere) for the SERS model in Figure 2(a) are given in Figure 2(d). The lines and asterisks represent the calculated results from rigorous generalized Mie theory and the 3D-FDTD method respectively. The solid and dashed lines correspond to situations with and without consideration of the size-dependent dielectric functions of the 10 nm Ag sphere. This figure attests an excellent agreement for the electromagnetic enhancement calculations between FDTD and Mie theory. The small difference (less than 5%), which is mainly caused by the staircase that approximates the spherical surface of the nanospheres in the FDTD calculation, can be expected to diminish if one uses a smaller Yee cell size. This result gives convincible evidence to show the validity and accuracy of the 3D-FDTD method in dealing with the problem of light scattering by metallic nanostructure in enhanced Raman scattering. Since FDTD is capable of performing electrodynamic calculations of light scattering from an object with any arbitrary shape, it is logical that this method is widely accepted and used in EM enhancement studies of complex SERS, TERS, HERS and SHINERS systems, especially for those consisting of non-spherical nanostructures or tips.

4 Non-uniform FDTD mesh method

3D-FDTD calculations often need very large memory resources for fine mesh in ERS simulations, which makes the calculation very time-consuming and expensive. In order to save the computation resources and calculation time for those ERS system with a big size, for example, a TERS geometry, one has to recur to the non-uniform FDTD mesh method [22,41]. The non-uniform mesh method makes it possible to take into account the precise geometric location of these interfaces using fine mesh cells in regions where the interfaces are important and larger mesh cells in bulk regions where there are no important interfaces as with homogeneous materials.

For example, the electromagnetic field enhancement in the surface of the single crystal substrate of a TERS geometry is mainly dependent on the near field coupling effect between the tip and substrate, and the size and shape of the tip's head plays another key effect in TERS enhancement factor except for the tip-substrate distance. Therefore in TERS FDTD simulations, the Yee cell size has to be small enough to accurately model both the tip's head and the gap between the tip and substrate. Taking account of the very small value (1 to 3 nm) of the tip-substrate distance in ordinary gap mode TERS configuration, the appropriate Yee cell size should be in the range of 0.5 to 1 nm. However, for simulating the real TERS experimental conditions, the length of the tip and the thickness and width of the substrate have to be in the order of several hundred nanometers. If a 1 nm × 1 nm × 1 nm or 0.5 nm × 0.5 nm × 0.5 nm Yee cell sized is adopted to mesh the total TERS configuration, the memory and system resources needed in the calculation will be immense, and the calculation time will be very long. Fortunately, the recently developed non-uniform mesh method in 3D-FDTD simulations has made great progress in saving computer resources and calculation time without losing accuracy [51].

Based on the non-uniform mesh 3D-FDTD method, we calculated the optical field enhancement in TERS geometry with and without a gold substrate, as shown in Figure 3(a)

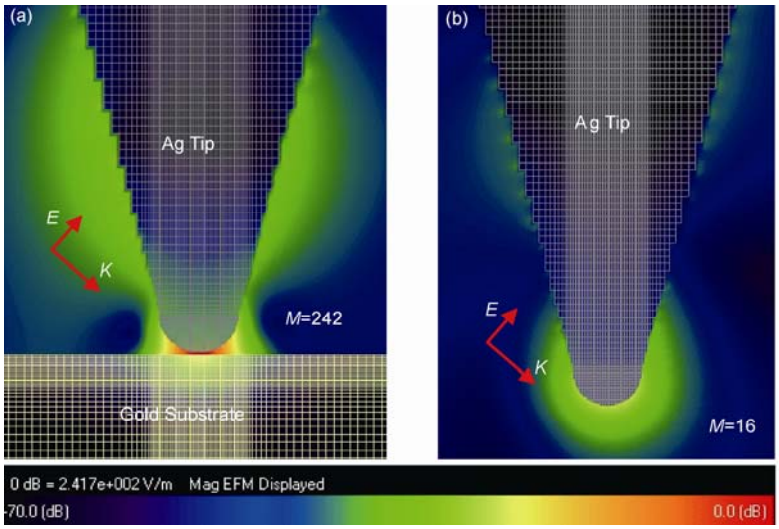

Figure 3 Non-uniform FDTD mesh method in TERS simulations. (a) FDTD simulations of electric field distribution for a silver tip held above a gold substrate; (b) FDTD simulations of electric field distribution for a single silver tip.

and (b). In the calculation, the silver tip is modeled as a metal cone with a radius of curvature 25 nm in both Figure 3(a) and (b). The 632.8 nm monochromatic plane wave is incident at an angle of $\pi/3$ measured from vertical direction, with the polarization in the plane of incidence, from the side. The distance between the tip and substrate in Figure 3(a) is set to be 2 nm. In the calculation, the Yee cell size in the head of the tip and the gap region was set to be 1 nm × 1 nm × 1 nm while 5 nm × 5 nm × 5 nm Yee cell size was used in other regions. This arrangement is rational since the enhancement factor is mainly decided by the fine nanostructure of the tip head and the tip-substrate distance. Figure 3(a) shows that the maximum field enhancement, defined as the ratio between the maximum local field and the incoming field amplitude, is about 242, which is much stronger than the field enhancement of 16 in a single tip (Figure 3(b)). Since the enhanced Raman scattering intensity from a probe molecule at any given position is approximately proportional to the fourth power of the electric field enhancement at the position of the molecule, the maximum Raman electromagnetic enhancement factor for the gap mode TERS is therefore 3.4×10^9. This huge EM enhancement is attributed to the strong near field coupling effect between the Ag tip and Au substrate. Therefore it is easy to understand that the maximum TERS enhancement in the same configuration decays almost 5 orders to 6.6×10^4 when the gold substrate is withdrawn.

It is important to keep in mind that the recommended ratio of 5:1 in Yee cell size between the smallest and largest cells in FDTD calculations should not be exceeded as this may affect the simulation accuracy [51]. In some cases, especially in ERS fields which involve the use of dispersive metallic materials, we have found that exceeding this limit will result in less accurate solutions.

5 Summary

We introduced the basic principles of 3D-FDTD and its application to enhanced Raman scattering spectroscopy which has, to date, contributed a great deal to the field of nanoplasmonics. The size-dependent dielectric functions of metallic nanoparticles are discussed in detail and the dependence of Ag dielectric constants on various sizes is given as an example. We illustrated the validity and accuracy of 3D-FDTD calculation in plasmonics field by comparing the FDTD results with rigorous Mie theory for the same SERS system. Our TERS calculation result showed that the non-uniform mesh method could save the computation resources greatly without losing accuracy if the technique is applied correctly.

We thank Kristen Delane Alexander for the valuable proofreading. This work was supported by the National Natural Science Foundation of China (20703032, 10625418, 10874233 and 10904171), the National Basic Research Program of China (2009CB930703, 2006DFB02020 and 2009CB930700), the Natural Science Foundation of Fujian Province of China (E0710028) and the Hundred Talents Project of Chinese Academy of Sciences.

1 Fleischmann M, Hendra P J, McQuillan A J. Raman spectra of pyridine adsorbed at a silver eletrode. Chem Phys Lett, 1974, 26: 163–166
2 Jeanmaire D J, Van Duyne R P. Surface Raman spectroelectrochemistry: Part I. Heterocyclic, aromatic, and aliphatic amines adsorbed on the anodized silver electrode. J Electroanal Chem, 1977, 84: 1–20
3 Albrecht M G, Creighton J A. Anomalously intense Raman spectra of pyridine at a silver electrode. J Am Chem Soc, 1977, 99: 5215–5217
4 Stockle R M, Suh Y D, Deckert V, et al. Nanoscale chemical analysis by tip-enhanced Raman spectroscopy. Chem Phys Lett, 2000, 318: 131–136
5 Anderson M S. Locally enhanced Raman spectroscopy with an atomic force microscope. Appl Phys Lett, 2000, 76: 3130–3132
6 Hayazawa N, Inouye Y, Sekkat Z, et al. Metallized tip amplification of near-field Raman scattering. Opt Commun, 2000, 183: 333–336
7 Brolo A G, Arctander E, Gordon R, et al. Nanohole-enhanced Rman scattering. Nano Lett, 2004, 4: 2015–2018
8 Bahns J T, Yan F, Qiu D, et al. Hole-enhanced Raman scattering. Appl Spectrosc, 2006, 60: 989–993
9 Li J F, Huang Y F, Ding Y, et al. Shell-isolated nanoparticle-enhanced Raman spectroscopy. Nature, 2009, 464: 392–395
10 Moskovits M. Surface-enhanced spectroscopy. Rev Mod Phys, 1985, 57: 783–826
11 Tian Z Q, Ren B, Li J F, et al. Expanding generality of surface-enhanced Raman spectroscopy with borrowing SERS activity strategy. Chem Commu, 2007, 34: 3514–3534
12 Wu D Y, Li J F, Ren B, et al. Electrochemical surface-enhanced Raman spectroscopy of nanostructures. Chem Soc Rev, 2008, 37: 1025–1041
13 Kneipp K, Wang Y, Kneipp H, et al. Single molecule detection using surface-enhanced Raman scattering (SERS). Phys Rev Lett, 1997, 78: 1667–1670
14 Nie S, Emory S R. Probing single molecules and single nanoparticles by surface-enhanced Raman scattering. Science, 1997, 275: 1102–1106
15 Xu H X, Bjerneld E J, Kall M, et al. Spectroscopy of single hemoglobin molecules by surface enhanced Raman scattering. Phys Rev Lett, 1999, 83: 4357–4360
16 Tian Z Q, Ren B, Wu D Y. Surface-enhanced Raman scattering: From noble to transition metals and from rough surfaces to ordered nanostructures. J Phys Chem B, 2002, 106: 9463 –9483
17 Pettinger B, Ren B, Picardi G, et al. Nanoscale probing of adsorbed species by tip-enhanced Raman spectroscopy. Phys Rev Lett, 2004, 92: 096101
18 Ren B, Picardi G, Pettinger B, et al. Tip-enhanced Raman spectroscopy of benzenethiol adsorbed on Au and Pt single-crystal surfaces. Angew Chem Int Ed, 2005, 44: 139–142
19 Moskovits M. Surface roughness and the enhanced intensity of Raman scattering by molecules adsorbed on metals. J Chem Phys, 1978, 69: 4159-4161
20 Li Q H, Yang Z L, Ren B, et al. The relationship between extraordinary optical transmission and surface-enhanced Raman scattering in subwavelength metallic nanohole arrays. J Nanosci nanotechnol, 2010, doi: 10.1166/jnn.2010.2911
21 Xu H X, Aizpurua J, Kall M, et al. Electromagnetic contributions to single-molecule sensitivity in surface-enhanced Raman scattering. Phys Rev E, 2000, 62: 4318–4324
22 Yang Z L, Aizpurua J, Xu H X. Electromagnetic field enhancement in TERS configurations. J Raman Spectrosc, 2009, 40: 1343–1348
23 Mie G. Beitrage zur optik truber medien seziell kolloidaler matallosungen. Ann Phys, 1908, 25: 377–455
24 Krug II J T, Sanchez E J, Xie X S. Design of near-field optical probes with optimal field enhancement by finite difference time domain electromagnetic simulation. J Chem Phys, 2002, 116: 10895–10902

25 Futamata M, Maruyama Y, Ishikawa M. Local electric field and scattering cross section of Ag nanoparticles under surface plasmon resonance by finite difference time domain method. J Phys Chem B, 2003, 107: 7607–7617
26 Oubre C, Nordlander P. Finite-difference time-domain studies of the optical properties of nanoshell dimers. J Phys Chem B, 2005, 109: 10042–10051
27 Tian Z Q, Yang Z L, Ren B, et al. Surface-enhanced Raman scattering from transition metals with special surface morphology and nanoparticle shape. Faraday Discuss, 2006, 132: 159–170
28 Chen Z H, Chu Q X. Stability analysis of the extended ADI-FDTD technique including lumped models. Sci China Ser F-Inform Sci, 2008, 51: 1607-1613
29 Kottmann J P, Martin O J F, Smith D R, et al. Dramatic localized electromagnetic enhancement in plasmon resonant nanowires. Chem Phys Lett, 2001, 341: 1–78
30 Micic M, Klymyshyn N, Suh Y D, et al. Finite element method simulation of the field distribution for AFM tip-enhanced surface-enhanced Raman scanning microscopy. J Phys Chem B, 2003, 107: 1574–1584
31 García de Abajo F J, Aizpurua J. Numerical simulation of electron energy loss near inhomogeneous dielectrics. Phys Rev B, 1997, 56: 15873–15884
32 García de Abajo F J, Howie A. Relativistic electron energy loss and electron-induced photon emission in inhomogeneous dielectrics. Phys Rev Lett, 1998, 80: 5180–5183
33 Hao E, Schatz G C. Electromagnetic fields around silver nanoparticles and dimers. J Chem Phys, 2004, 120: 357–366
34 Qin L D, Zou S L, Xue C, et al. Designing, fabricating, and imaging Raman hot spots. Proc Natl Acad Sci USA, 2006, 103: 13300–13303
35 Ozbay E. Plasmonics: Merging photonics and electronics at nanoscale dimensions. Science, 2006, 311: 189–193
36 Oubre C, Nordlander P. Optical properties of metallodielectric nanostructrues calculated using the finite difference time domain method. J Phys Chem B, 2004, 108: 17740–17747
37 Maier S A, Kik P G, Atwater H. Observation of coupled plasmon-polariton modes in Au nanoparticle chain waveguides of different lengths: Estimation of waveguide loss. Appl Phys Lett, 2002, 81: 1714–1716
38 Kik P G, Maier S A, Atwater H. Image resolution of surface-plasmon-mediated near-field focusing with planar metal films in three dimensions using finite-linewidth dipole sources. Phys Rev B, 2004, 69: 045418
39 Li Z, Gong Q H. The plasmonic coupling of metal nanoparticles and its implication for scanning near-field optical microscope characterization. Chinese Sci Bull, 2009, 54: 3843–3843
40 Yee K. Numerical solution of initial boundary value problems involving Maxwell's equations in isotropic mediam. IEEE Trans Antennas Propag, 1966, 14: 302 –307
41 Kunz K S, Luebbers R J. The Finite Difference Time Domain Method for Electromagnetics. Boca Raton: CRC Press LLC, 1993
42 Luebbers R J, Hunsberge F, Kunz K S. A frequency-dependent finite-difference time-domain formulation for transient propagation in plasma. IEEE Trans Antennas Propag, 1991, 39: 29–34
43 Bian R X, Dunn R C, Xie X S, et al. Single molecule emission characteristics in near-field microscopy. Phys Rev Lett, 1995, 75: 4772–4775
44 Tian Z Q, Yang Z L, Ren B, et al. Surface-enhanced Raman scattering. Topics Appl Phys, 2006, 103: 125–146
45 Kreibig U, Vollmer M. Optical Properties of Metal Clusters. Berlin: Springer, 1995
46 Coronado E A, Schatz G C. Surface plasmon broadening for arbitrary shape nanoparticles: A geometrical probability approach. J Chem Phys, 2003, 119: 3926–3934
47 Xu H X. Comment on "Theoretical study of single molecule fluorescence in a metallic nanocavity". Appl Phys Lett, 2005, 87: 066101
48 Li Z P, Yang Z L, Xu H X. Comment on "Self-similar chain of metal nanospheres as an efficient nanolens". Phys Rev Lett, 2006, 97: 079701
49 Johnson P B, Christy R W. Optical constants of the noble metals. Phys Rev B, 1972, 6: 4370–4379
50 Li K, Stockman M I, Bergman D J. Self-similar chain of metal nanospheres as an efficient nanolens. Phys Rev Lett, 2003, 91: 227402
51 XFDTD reference manual. Version 6.3. Remcom Inc, 2004